J. Opt. A: Pure Appl. Opt. **11** (2009) 015503 (8pp) doi:10.1088/1464-4258/11/1/015503

Precision *in situ* volume measurement of micro droplets

Kuang-Chao Fan[1], Jhih-Yuan Chen[1], Ching-Hua Wang[1] and Wen-Chueh Pan[2]

[1] Department of Mechanical Engineering, National Taiwan University, 1, Section 4, Roosevelt Road, Taipei 106, Taiwan, Republic of China
[2] Chung Shan Institute of Science and Technology, PO Box 90008-15-3, Lung-Tan, Tao-Yuan 32526, Taiwan, Republic of China

E-mail: fan@ntu.edu.tw

Received 24 July 2008, accepted for publication 4 November 2008
Published 5 December 2008
Online at stacks.iop.org/JOptA/11/015503

Abstract
This research presents an *in situ* droplet volume measurement system which is applied to the one drop fill (ODF) process of liquid crystal display (LCD) manufacture. The system developed utilizes a stroboscopic technique to synchronize the triggering of a strobe light and a CCD camera. A steady image of the droplet flying in free space can be captured *in situ* by the CCD camera. The method of precise volume estimation is based on a rotationally symmetric model of the droplet's shape. Polynomial fitting is used to reconstruct the droplet profile. The image resolution can thus be enhanced by a subpixel technique. Compared to a precision electronic balance, the total weight measured by this system has an error within ±0.3%, and the computation time for each droplet is about 0.4 s. This satisfies the actual ODF requirements.

Keywords: one drop fill, micro droplet, volume measurement, image processing

(Some figures in this article are in colour only in the electronic version)

1. Introduction

When a liquid crystal display (LCD) panel size is beyond the fifth generation (1120 mm × 1250 mm), the liquid crystal (LC) filling process undergoes a technological change, namely the one drop fill (ODF) technology, which replaces the conventional injection method between two glass substrates by dispensing micro drops onto the bottom substrate and subsequently pressing down the upper substrate. The key to ODF technology is to use a dispenser to control the amount of LC deposited on the substrate. If the total amount of LC is less or more than the required volume, this would cause an uneven distribution of the LC between the two substrates and result in uneven brightness of the LCD, which is called a Mura defect [1, 2]. In order to accurately detect the amount of LC dispensed onto the substrate, the common method is to measure the weight of a certain amount of drops with a precision electronic balance. Using an electronic balance to calibrate the drop volume has at least the following three disadvantages: (1) it is not a single droplet measurement: the drops distributed around the substrate may have varying sizes; (2) the volume of a single LC drop is not the actual volume but an averaged volume; (3) after several repetitions of ODF processes, the weight measurement must be re-calibrated in order to ensure that the dispenser controller remains within normal conditions. An accurate and low-cost drop-on-demand droplet generator for the ODF process with an *in situ* image measurement system has been developed by the authors [3]. This research continues the work of precise measurement of a single droplet volume, using the proposed image processing technique. The technique of precise shape detection of the droplet is the key problem to be solved.

There are many basic techniques dealing with shape detection by image processing, such as threshold selection [4, 5] and edge detection. Canny [6] proposed an optimal edge detection algorithm, which can efficiently reduce the noise in two dimensions. It is understood that the noise would be amplified were we to use the object's two-dimensional (2D) image to calculate its 3D volume because the accuracy of the edge detection will significantly affect the 3D volume calculated. Furthermore, when a droplet is flying in the air, its shape will be distorted by external forces, such as gravity,

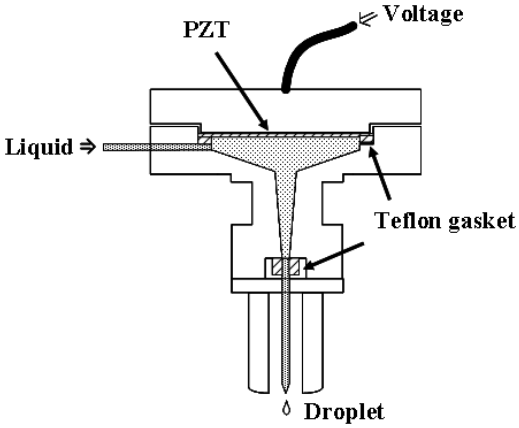

Figure 1. Assembly of the droplet generator.

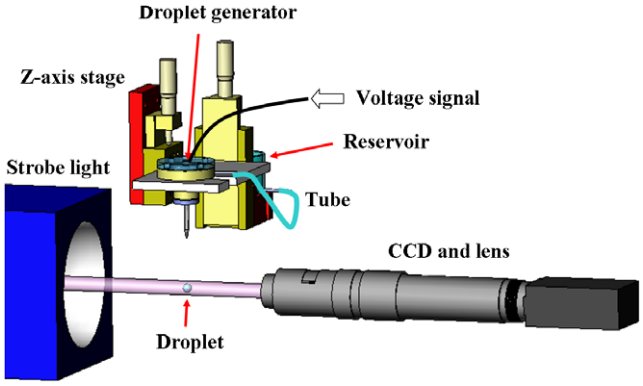

Figure 2. *In situ* measurement system.

surface tension and air resistance. Most drops show a shape variation along the vertical direction. Therefore, the location of the captured image and the volume calculation method are important for this research.

Hugli compared three volume models of the droplet image: (1) a spherical model, (2) an ellipsoidal model, and (3) an arbitrary rotational symmetric model [7]. The first two models have larger estimation errors because the droplet shape is not a perfect sphere or a perfect ellipsoid. The third model is easy to use, but does not yield a high precision of the calculated volume due to the difficulty of finding the axis of rotation as well as the limitations of pixel resolution. Shape recovery is a major problem that merges two or three 2D images into one 3D image. The method used is called shape from shading (SFS) [8, 9]. It requires more than one CCD camera to capture images of a moving object in time. However, if the shape is of a rotational symmetric type, the volume can be constructed from a model of a solid of revolution [10]. Lynch *et al* [11] use the cylindrical shells volume integral to conceptualize a tree stem as being a solid of revolution. Although the form of a continuous integral can avoid the estimation error caused by a discrete approximation of the integral, the precise location of the axis is difficult to obtain.

In the case of a continuous dispensing droplet, the *in situ* measurement system developed depends critically on the image processing runtime and the accuracy of the volume estimation algorithm. The first part of this report shows how to construct an image data structure in order to improve the image processing runtime. The second part describes the volume estimation method by integration of cross-sectional areas. The software is developed using Microsoft Visual C^{++} 6.0. The hardware adopts the same *in situ* measurement system as previously reported by the authors [3] and Kamiya *et al* [12].

2. Experimental set-up

There are several types of droplet generator, such as the squeeze mode [13], the shear mode [14], the bend mode [15], and the push mode [16]. For designing the simple structure of a low-cost droplet generator, we use a disk type piezoelectric buzzer as the driving source and the bend mode of the PZT motion to apply a pushing force to the contained liquid.

2.1. The in situ measurement system

Figure 1 shows the assembly of the droplet generator. The PZT actuator is taken from the piezoelectric buzzer of a commercially available speaker. It is constructed of a thin piezo-ceramic layer, about 0.2 mm thick, which is stuck on a vibration diaphragm with a diameter of 27 mm. The actuator is fixed to the upper side of the main body. When a voltage pulse is applied to the PZT, the diaphragm will bend, and a pressure pulse is generated in the liquid flow channel to push a certain amount of liquid out of the glass nozzle. The liquid in the chamber can entirely be sealed by Teflon gaskets. Four stoppers surrounding the nozzle protect it from collision breakage.

The *in situ* measurement system is composed of a CCD camera, a zoom lens, and a stroboscopic light, as shown in figure 2. The strobe light is simultaneously triggered by the same frequency as the function generator which actuates the PZT film. By selecting a proper shutter speed, a steady image of the droplet can clearly be viewed and captured by the camera. The vision system is composed of a high-resolution (1024 $\times$ 760 pixels) CCD camera, a 4$\times$ TV extender and a 7$\times$ zoom lens. The working distance is 900 mm and the field of view is 800 μm $\times$ 600 μm. In this study, the measured droplet is assumed to be a moving object. Thus, if the time of exposure is too long, the edge will be blurred. We set the time of CCD exposure to 20 μs; the brightness and the contrast are both adjusted on demand.

2.2. Image processing

Before estimating the volume of the drop, the captured image has to be processed by several image processing techniques. The techniques we used are Canny edge detection [6], Gaussian filtering, and point clustering. Finally, the remaining pixels form the edge of the droplet, as shown in figure 3.

2.3. CCD camera calibration

In general, there are two factors that will cause errors in finding the drop edge. The first is related to the image processing described above. The second is related to the CCD camera calibration. We have to know the

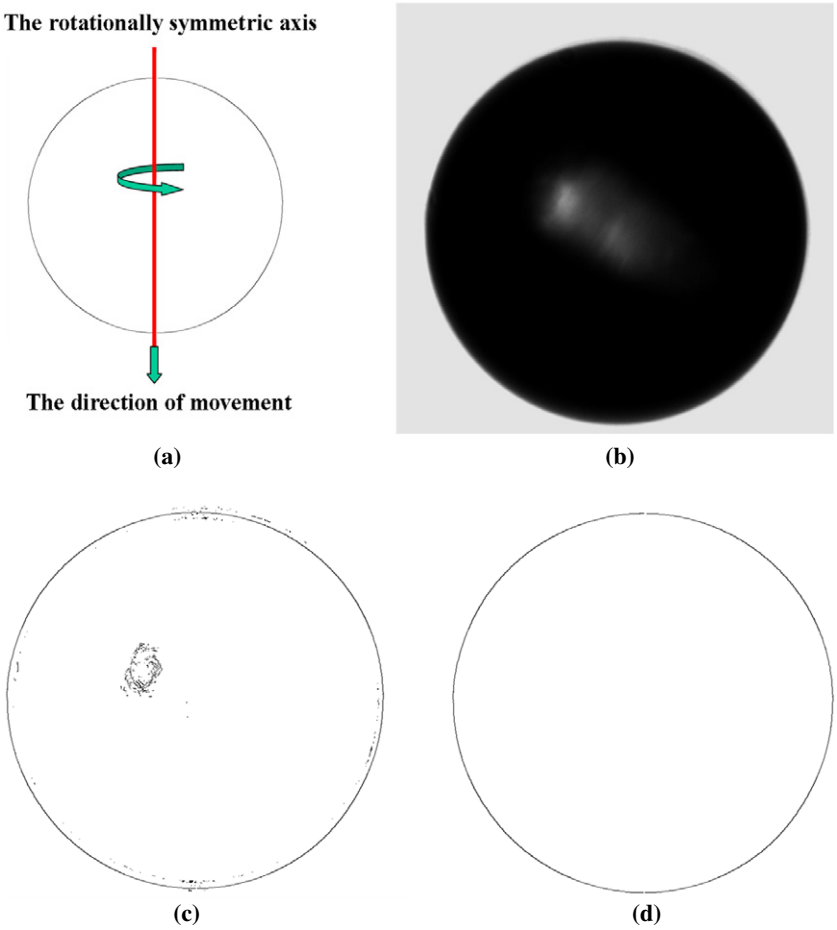

Figure 3. Image processing: (a) a schematic diagram of a droplet flying in free space, (b) original droplet image, (c) after edge detection, (d) after filtering and clustering.

actual dimension represented by a single pixel and obtain the calibration parameters affected by lens distortion and coordinate transformation. Tsai [17] proposed a method for CCD camera calibration that was used to determine the actual dimension in an image coordinate system. Because this method has to know the geometry location of the CCD camera, it is time consuming and is not suitable for a high-speed measurement system.

In this study, we used the mapping function method [18, 19] to derive the relationship between the measuring plane coordinate and the image coordinate. Any point located on the measuring plane can be mapped to a pixel located on the image by a mapping function. The mapping function is defined by

$$\begin{aligned} X &= a_1u^2 + b_1uv + c_1v^2 + d_1u + e_1v + f_1 \\ Y &= a_2u^2 + b_2uv + c_2v^2 + d_2u + e_2v + f_2, \end{aligned} \tag{1}$$

where (X, Y) is the measuring plane coordinate, and (u, v) is the corresponding image coordinate.

Regression analysis was used to solve the coefficients of the mapping function. A mask pattern, with 0.5 μm dimensional accuracy, was used to calibrate the CCD camera, as shown in figure 4. The actual locations of the corner points of each pattern are known as reference points on the (X, Y) plane. The corresponding pixels of the corner points in the (u, v) image plane can be mapped precisely by least squares line fitting for finding the intersection point of two edges. After calibration in a selected region of 500 μm $\times$ 500 μm, the average accuracy is within 0.5 μm. The derived coefficients are given in table 1.

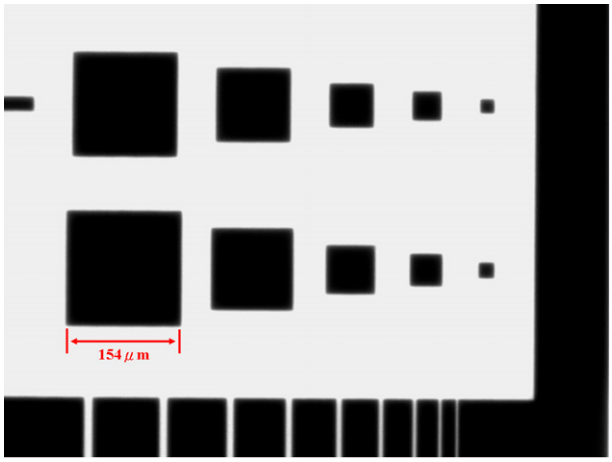

Figure 4. Calibration mask pattern.

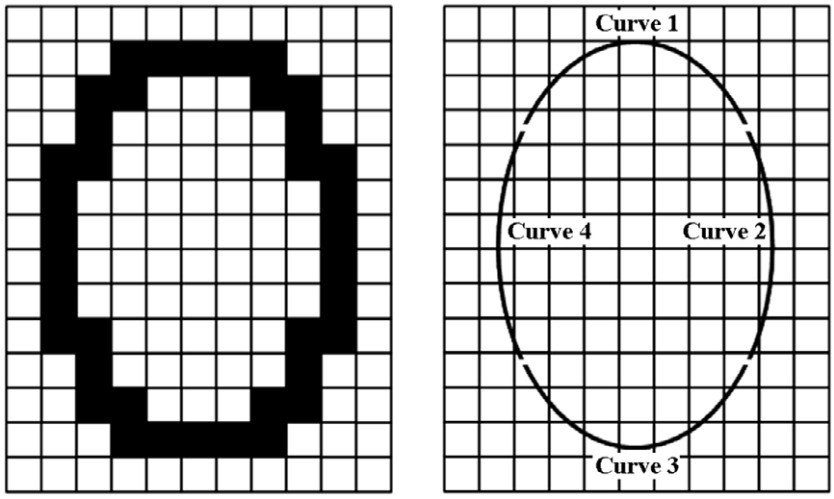

Figure 5. (a) The captured image. (b) The edge points are fitted by four appropriate curves.

Table 1. Coefficients of mapping function.

Coefficients	
$a_1 = 0.000\,001$	$a_2 = 0.000\,000$
$b_1 = -0.000\,004$	$b_2 = 0.000\,000$
$c_1 = 0.000\,003$	$c_2 = -0.000\,005$
$d_1 = 0.781\,914$	$d_2 = -0.043\,746$
$e_1 = 0.045\,357$	$e_2 = 0.785\,122$
$f_1 = -234.824\,707$	$f_2 = -56.220\,375$

3. Reconstruction of the droplet profile by polynomial curve fitting

Since the resolution of the CCD and the magnification of the lens are both limited, edge detection by a single-pixel resolution will certainly produce discrete errors compared to the real edge. In order to obtain the edge pixels with a low error, subpixel edge detection is an important technique for improving the measurement accuracy [20–22].

Because of the surface tension, gravity and air resistance effects, the droplet shape is not a perfect sphere or ellipsoid, but it can at least be assumed to be a symmetrical shape along the direction of movement. Any horizontal cross section of the droplet can thus be regarded as a perfect circle. Suppose that figure 5(a) is a captured image, and its unit is one pixel. The contour of the flying droplet will remain a continuous and smooth curve for a short time after leaving the dispenser nozzle. It is not accurate enough to describe a rotationally symmetric droplet by just a single polynomial function. Therefore, we divide the drop edge into four independent curves, as shown in figure 5(b).

Curves such as cubic functions, B-splines and polynomials are often used to fit discrete points. Since the image pixels are distributed in a stepwise form, the fitting curve will have small local residues if cubic functions or B-splines are used. In our research, we use polynomials to fit the drop edge by the least squares method. Suppose there are totally N measured edge points and each point i has the image coordinates (u_i, v_i). Then the general form of a polynomial is given by

$$f(u) = \sum_{k=0}^{M-1} a_k u^k. \tag{2}$$

The sum of the squared errors is defined by

$$\chi^2 = \sum_{i=0}^{N-1} \left[\frac{v_i - \sum_{k=0}^{M-1} a_k u_i^k}{\sigma_i} \right]^2, \tag{3}$$

where M is the polynomial order, a_k the coefficient of the kth order and σ_i the standard deviation of the ith data point. We can find the optimal coefficients that minimize χ^2 by differentiation with respect to each of the coefficients as below.

$$\frac{\partial \chi^2}{\partial a_k} = \sum_{i=0}^{N-1} \frac{1}{\sigma_i^2} \left[v_i - \sum_{k=0}^{M-1} a_k u_i^k \right] \left[\frac{\partial (\sum_{k=0}^{M-1} a_k u_i^k)}{\partial a_k} \right] = 0. \tag{4}$$

Equation (4) yields

$$0 = \sum_{i=0}^{N-1} \frac{1}{\sigma_i^2} \left[v_i - \sum_{k=0}^{M-1} a_k u_i^k \right] u_i^k. \tag{5}$$

Equation (5) can be simplified to

$$\sum_{k=0}^{M-1} \alpha a_k = \beta, \tag{6}$$

where

$$\alpha = \sum_{i=0}^{N-1} \frac{u_i^{2k}}{\sigma_i^2} \tag{7}$$

is an $M \times M$ matrix, and

$$\beta = \sum_{i=0}^{N-1} \frac{v_i x_i^k}{\sigma_i^2} \tag{8}$$

is a vector of length M. The optimal parameters can be calculated from

$$a_k = \sum_{k=0}^{M-1} [\alpha]^{-1} \beta. \tag{9}$$

In this study, we used a standard circle to calibrate the polynomial curves. Each curve was fitted by a seventh-order polynomial after χ^2 converged to a specified value.

4. Image data structure

For image processing, a blob is defined as a region of connected pixels. Blob analysis is the identification and study of this image region. A common method, called eight-connectivity, is that each pixel has eight adjacent pixels along the vertical, horizontal and diagonal axes. If the pixels have the same gray level, such as black or white, we can group them together and establish the connectivity between them. But the connectivity will be lost after using a subpixel technique, and this will increase the complexity of image processing. In this study, we construct an image data structure to establish the connectivity of the pixels and speed up the search process of the image data.

4.1. Cell subdivision

The purpose of this study is to provide an algorithm based on a cell subdivision for storing and searching of image data. Cell subdivision is based on the idea that the bounding area of a point group is divided into subcells, and it assigns each point to a suitable subcell [23]. The cell subdivision algorithm is suitable for grouping of discrete data. Although the pixels within one subcell have similar characteristics, the number of pixels is still limited by the resolution of the CCD. So, we have to combine the subpixel method and the cell subdivision algorithm in order to increase the measurement accuracy and reduce the runtime of the application.

The numbers of original pixels along the image coordinates (u, v) are k and l, respectively. To divide each pixel into $n \times n$ parts, the total number of subcells in an image will be $n^2 \times k \times l$, as shown in figure 6. The region number of any subpixel point $P(u, v)$ located in a subcell is defined by the following indices.

$$\begin{aligned} \text{index\_}v &= \text{int}(v \times n) \\ \text{index\_}u &= \text{int}(u \times n). \end{aligned} \tag{10}$$

Grouping the points in subcells can really overcome the shortcoming of an insufficient resolution and help to establish the connectivity of points. The total memory, however, will greatly increase, and the application runtime will increase about n^2 times for searching all subcells. According to the demands of an *in situ* fast measurement system, it is necessary to establish an image data structure for quick storing and searching of the image data.

4.2. Storing and searching of subpixel points

The points within a subcell are generally unstructured, and they are stored without any connectivity. An image data structure is thus established for storing and searching of these data. Searching is one of the fundamental computational tasks for retrieving particular information from a large amount of stored information. In this work, we used a hashing function and a standard template library (STL) to establish the image data structure.

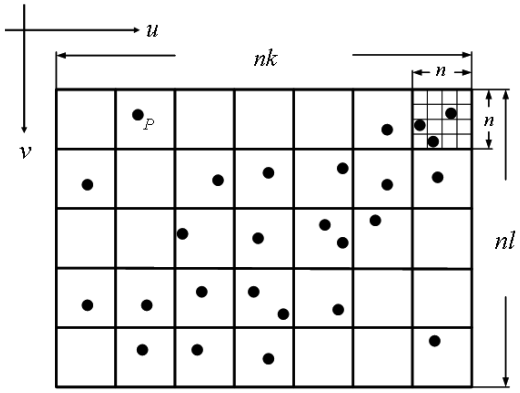

Figure 6. Division of each pixel into $n \times n$ parts.

Hashing [24] is widely used in computer graphics to locate close pairs of points in a 2D plane or in a 3D space. We have to define a hash function which can be used to map a key value to an index in the hash table, where the corresponding record is stored. A good hash function also should not produce the same index for two different keys. Otherwise, this is known as a collision. The advantage of using a hash table is that the search speed is not related to the amount of data and the data in the hash table will not collide. The hash table, similar to the memory space, should be established before storing the data. If there is not enough memory space, this is called an overflow. In this study, we use the associate container provided by the STL, a software library written in Visual C^{++} 6.0, to establish a hash table. The advantage of adopting an STL is that the size of the associate container can be dynamically adjusted with respect to the amount of data. This can significantly save memory space and automatically avoid overflow.

The associate container allows mapping from an index value to a datum. Because the index values calculated by the hashing function should avoid any collision, we have to design the hashing function carefully when the amount of data is large. The index of each subpixel is defined by

$$\text{Index}(u, v) = \text{index\_}u + n \times k \times \text{index\_}v. \tag{11}$$

The image data structure is shown in figure 7. Each pixel has three recorded data: flag, number of subpixels, and pointer. The flag of each pixel indicates whether the subpixel data are contained in the cell. If there are subpixel points stored in the cell, the number of subpixels is increased and the pointer directly refers to another address of the computer memory. The algorithm to establish the image data structure is as follows.

(i) Index value: the subpixel points are filled into the subcells, and then each key value is mapped by the hashing function to an index in the hash table.
(ii) Flag state: there are two states of the flag, true and false, to judge whether the data are contained within the cell. It saves much time finding subpixel points without searching empty subcells.

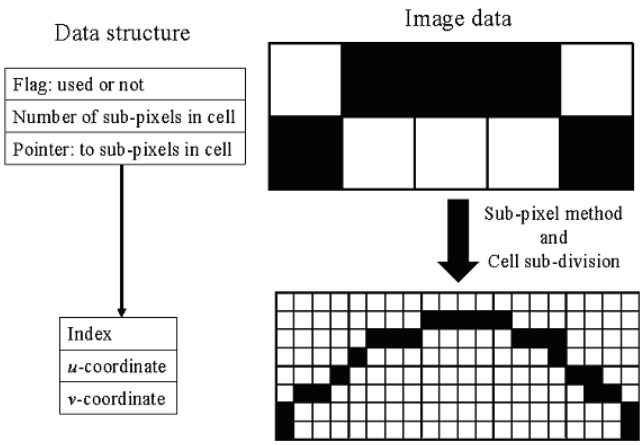

Figure 7. Image data structure.

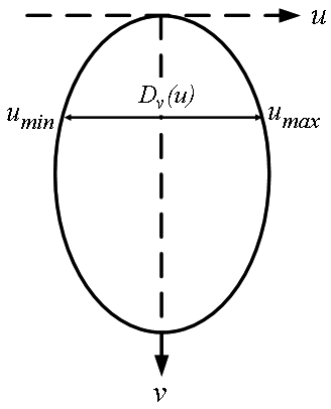

Figure 8. The rotationally symmetric model.

(iii) Storing subpixel data: the coordinates of subpixel points and their corresponding index values are stored in the associate container. If there are more than two points located in one subcell, we will calculate the center coordinates of these two points and replace these two points by the center point. Finally, every index value is unique and no collision will occur.

5. The drop volume estimation

Since the droplet shape is not a perfect sphere or ellipsoid, the drop volume estimation is based on the concept of a rotationally symmetric model [7]. The subpixel technique is applied to reduce the error of the estimated volume caused by the discrete approximation.

5.1. Estimating the rotationally symmetric volume

The rotationally symmetric model is based on the assumption that the cross section of the droplet along the vertical direction is a perfect circle, as shown in figure 8. The volume can be estimated by the discrete approximation

$$V = \frac{\pi}{4}\left(\sum_{v=0}^{v_{\max}} D_v^2(u)\right) \qquad D_v(u) = (u_{\max} - u_{\min})_v, \quad (12)$$

where $D_v(u)$ is the diameter of the cross section at position v, and $u_{\max}$ and $u_{\min}$ are the detected edge positions along the u direction.

The accuracy of the volume estimation depends on the pixel size, which is limited by the resolution of the CCD. The measurement accuracy is improved by the method of subpixel interpolation described as follows.

5.2. Subpixel interpolation

In order to reduce the estimation error caused by the discrete approximation of the integral, we have to increase the number of tomographic sections of the droplet. Firstly, the edge curve fitted by the polynomial function is thinned in the horizontal direction to subpixel points. The vertical sectioning is also interpolated with the same subpixel resolution. Secondly, the subpixel points are filled into the subcells by a cell subdivision algorithm. Finally, an index number is assigned to each subpixel. In this study, having considered the avoidance of collision and overflow, each pixel is divided into 10 × 10 subcells.

Table 2. Results of the three edge processing methods.

	Roundness (pixel)	Calculated volume (pixel^3)	Volume error (%)
Method 1	1.219	112 387 377	0.055
Method 2	0.15	112 336 009	0.009
Method 3	0.137	112 335 592	0.009

5.3. Tests of the subpixel method

The test is simulated by generating an ideal circle of 299.316 pixels in diameter in the image. With the least squares circle fitting method, the estimated volume is 112 325 399 pixel^3. In this study, we compare the results of three edge processing methods and use the roundness value to assess the accuracy. These three drop volume estimation methods are all based on the rotationally symmetric model.

(i) *Method 1*. The edge points are detected by the Canny method to a resolution of one pixel.
(ii) *Method 2*. From the Canny method, the edge of the circle is divided into four sections. Each section is fitted by a polynomial curve. Then the curve points are processed by the proposed subpixel method and recorded by the proposed image data structure.
(iii) *Method 3*. Considering the continuity problem between the boundaries of those four curves, we refit a new polynomial curve across each corresponding boundary to smooth out the discontinuities. The original edge points are replaced by new points generated by the new polynomial curve, as shown in figure 9.

The results are listed in table 2. Methods 2 and 3 show almost the same volume estimation error, which is much better than that of method 1. Although method 3 has a

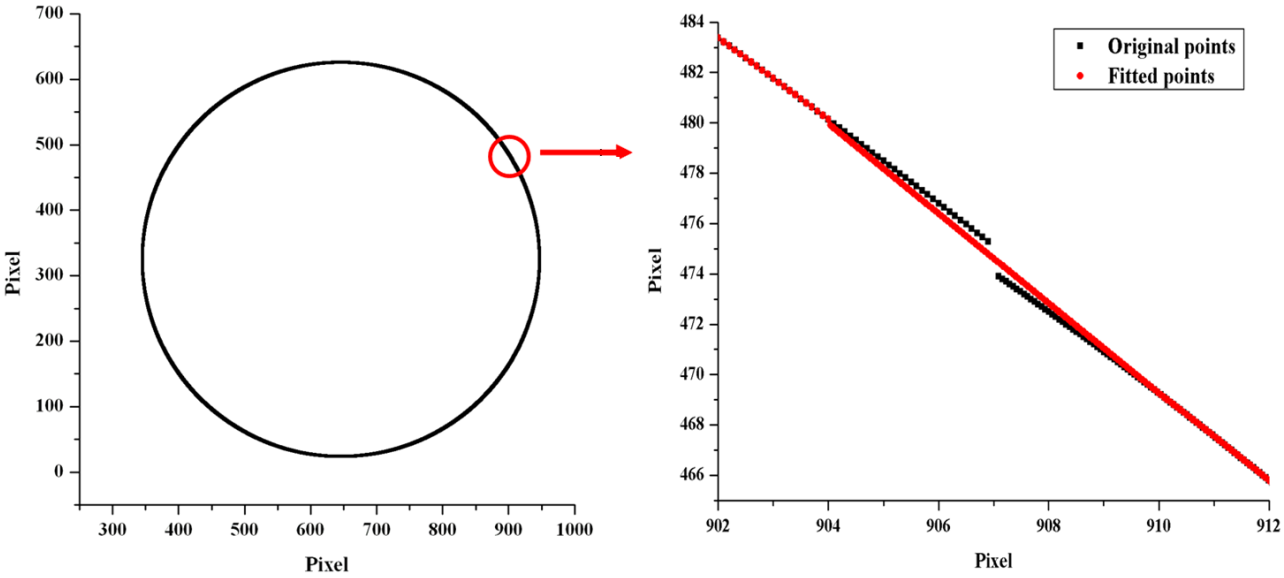

Figure 9. Smooth fitting of the boundary points.

Table 3. Test results of the application runtime.

Item	Search all n^2 subcell array	Search hash table
Memory usage	500 MB	80 MB
Image processing	0.141	0.141
Edge data processing	0.218	0.146
Volume calculation	0.235	0.01
Runtime of total drops		
10	15.45	3.64
50	68.23	19.31
100	134.76	40.96
500	683.62	207.87
1000	1250.06	402.96
Unit Images	Sec	Sec

smaller roundness value, it takes more computational time. Considering the fast *in situ* computation requirement of this study, method 2 will be the best choice.

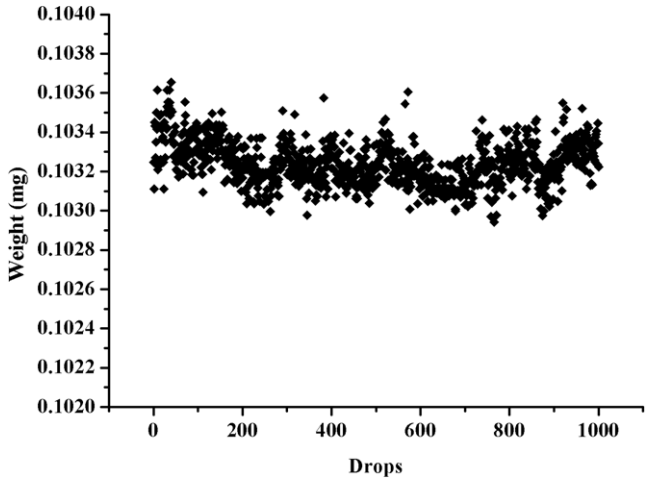

Figure 10. Measured weights of 1000 drops by the subpixel method.

6. Experimental results

6.1. Application runtime

The hardware used is a 2.8 GHz Pentium 4 CPU, and the memory space is 1.5 GB. The results of the runtime tests are listed in table 3. It can clearly be seen that, by establishing a hash table with an n^2 subcell array of each pixel, the application runtime can be significantly reduced to one third. The time is mainly spent on the edge data processing, which includes the polynomial curve fitting and the data storage. The volume calculation time is negligible for the proposed method and its memory usage is largely reduced.

6.2. Drop volume measurement

The liquid tested is a liquid crystal (Chisso Co., Model ZOC-5114LA) with a density of 1.06 g cm^{-3}. The experimental data of the total weight of the drops from ten measurements are determined after accumulating 1000 drops in each measurement. The above-mentioned method 1 and method 2 are compared, namely the original edge pixel method and the edge subpixel method. The measured results are compared with a reference weight determined by an electronic balance (A&D Co., Model HR-200), as listed in table 4. The measurement errors of the subpixel method are all within $\pm 0.3\%$, while the pixel method shows errors that are too large. The detailed weight data of measurement 1 of the subpixel method are plotted in figure 10. Every droplet is well controlled to within $\pm 0.3\%$ weight deviation.

7. Conclusions

This report introduces a high-precision volume measurement vision system for a single micro droplet flying in free space.

Table 4. Measurement errors of ten experiments.

	Measurement										
Method	1	2	3	4	5	6	7	8	9	10	Unit
1	6.14	10.4	8.87	6.33	4.42	4.39	9.4	7.8	0	7.5	‰
2	0.8	2.61	1.01	1.95	0.21	0.1	2.4	0.16	−2.4	0.8	‰

The liquid profile is fitted by four segmented polynomial curves after edge detection. A 10×10 subdivision algorithm is proposed to increase the image resolution. The coordinates of subpixel points and their corresponding index values are stored in an associate container by using a hash table. This image data structure can significantly reduce the runtime and the stored memory. Experimental results show that using four seventh-order polynomial curves to fit the drop edge can assure a high accuracy of the drop volume measurement. The measurement errors of a single drop and of accumulated drops are all within $\pm 0.3\%$. Although it is primarily designed for ODF purposes, this measurement system can also be applied to measuring any other small drop volume *in situ*.

Acknowledgment

The authors gratefully acknowledge the support of the Chung-Shan Institute of Science and Technology for this work, through Grant No. BB97006P.

References

[1] Mori Y, Tanahashi K and Tsuji S 2004 Quantitative evaluation of 'mura' in liquid crystal displays *Opt. Eng.* **43** 2696–700
[2] Kweon H J and Son H J 2005 Apparatus for measuring dispensing amount of liquid crystal drops and method for manufacturing liquid crystal display device using the same *US Patent Specification* 6,864,948
[3] Fan K C, Chen J Y, Wang S H and Pan W J 2008 Development of a drop-on-demand droplet generator for one-drop-fill technology *Sensors Actuators* A **147** 649–55
[4] Otsu N 1979 Threshold selection method from gray-level histograms *IEEE Trans. Syst. Man Cybern.* **9** 62–6
[5] Sahoo P K, Soltani S, Wong A K C and Chen Y C 1988 Survey of thresholding techniques *Comput. Vis. Graph. Image Process.* **41** 233–60
[6] Canny J 1986 Computational approach to edge detection *IEEE Trans. Syst. Man Cybern.* **PAMI-8** 679–98
[7] Hugli H and Gonzalez J 2000 Drop volume measurements by vision *Proc. SPIE—Int. Soc. Opt. Eng.* **3966** 60–6
[8] Horn B K P 1987 *The Psychology of Computer Vision* ed P H Winston (New York: McGraw-Hill) pp 115–55
[9] Bakhtiyarov S, Dupac M and Overfelt R A 2006 Shape recovery of a levitated aspherical droplet from 2D image information *Trans. ASME J. Fluids Eng.* **128** 463–6
[10] Harris J W and Stocker H 1998 *Handbook of Mathematics and Computational Science* (New York: Springer) pp 111–3
[11] Lee H and Han S 2005 Reconstruction of 3D interacting solids of revolution from 2D orthographic views *Comput. Aided Des.* **37** 1388–98
[12] Kamiya H, Suh D J and Jeon B K 2006 System and method for detecting dropping amount of liquid crystal *US Patent Specification* 20060151727
[13] Shore H J and Harrison G M 2005 The effect of added polymers on the formation of drops ejected from a nozzle *Phys. Fluids* **17** 033104
[14] Brunahl J and Grishin A M 2002 Piezoelectric shear mode drop-on-demand inkjet actuator *Sensors Actuators* A **101** 371–82
[15] Laurell T, Wallman L and Nilsson J 1999 Design and development of a silicon microfabricated flow-through dispenser for on-line picolitre sample handling *J. Micromech. Microeng.* **9** 369–76
[16] Tamai S 2005 Liquid crystal dropping apparatus and method, and liquid crystal display panel producing apparatus *US Patent Specification* 6,851,460
[17] Tsai R Y 1987 A versatile camera calibration technique for high-accuracy 3D machine vision metrology using off-the-shelf TV cameras and lenses *IEEE J. Robot Autom.* **3** 323–44
[18] Tai W C and Chang M 1996 A machine vision technique for subpixel estimation of three-dimensional profilometry *Opt. Quantum Electron.* **28** 1571–82
[19] Fan K C, Lee M Z and Mou J I 2002 On-line non-contact system for grinding wheel wear measurement *Int. J. Adv. Manuf. Technol.* **19** 14–22
[20] Shan Y and Boon G W 2000 Sub-pixel location of edges with non-uniform blurring: a finite closed-form approach *Image Vis. Comput.* **18** 1015–23
[21] Truchetet F, Nicolier F and Laligant O 2001 Subpixel edge detection for dimensional control by artificial vision *J. Electron. Imaging* **10** 234–9
[22] Qu Y D, Cui C S, Chen S B and Li J Q 2005 A fast subpixel edge detection method using Sobel–Zernike moments operator *Image Vis. Comput.* **23** 11–7
[23] Fang T P and Piegl L A 1995 Delaunay triangulation in three dimensions *IEEE Comput. Graph. Appl.* **15** 62–9
[24] Vanco M, Brunnett G and Schreiber T 1999 A hashing strategy for efficient k-nearest neighbors computation *Proc. Computer Graphics Int. 1999* ed G Brunnett, pp 120–8